Available online at www.sciencedirect.com

ScienceDirect

journal homepage: www.elsevier.com/locate/he

# Evaluation of $Ni_{80}Cr_{20}/(La_{0.75}Sr_{0.25})_{0.95}MnO_3$ dual layer coating on SUS 430 stainless steel used as metallic interconnect for solid oxide fuel cells

*Wei Wu, Wanbing Guan**, Guoliang Wang, Wu Liu, Qingsheng Zhang, Tao Chen, Wei Guo Wang**

*Ningbo Institute of Material Technology and Engineering, Chinese Academy of Science, 519 Zhuangshi Road, Zhenghai District, CN-315201, Ningbo, PR China*

ARTICLE INFO

*Article history:*
Received 21 August 2013
Received in revised form
14 October 2013
Accepted 16 October 2013
Available online 4 December 2013

*Keywords:*
Metallic interconnect
Coating
Area specific resistance
Stack
Solid oxide fuel cell

ABSTRACT

$Ni_{80}Cr_{20}/(La_{0.75}Sr_{0.25})_{0.95}MnO_3$ dual-layer coating is deposited on SUS 430 alloy by plasma spray for solid oxide fuel cell (SOFC) interconnect application. The phase structure, area specific resistance (ASR), and morphology of the coating are studied. A two-cell stack is also assembled and tested to evaluate coating performance in an actual SOFC stack. The NiCr/LSM coating adheres well to the SUS 430 alloy after oxidation in air at 800 °C for 2800 h. The ASR and its increasing rate of coated alloy are 25 mΩ $cm^2$ and 0.0017 mΩ $cm^2$/h, respectively. In an actual stack test, the maximum output power density of the stack repeating unit increases from 0.32 W $cm^{-2}$ to 0.45 W $cm^{-2}$ because of the application of NiCr/LSM coating. The degradation rate of the stack repeating unit with no coating is 4.4%/100 h at a current density of 0.36 A $cm^{-2}$, whereas the stack repeating unit with NiCr/LSM coating exhibits no degradation. $Ni_{80}Cr_{20}/(La_{0.75}Sr_{0.25})_{0.95}MnO_3$ dual-layer coating can remarkably improve the thermal stability and electrical performance of metallic interconnects for SOFCs.



## 1. Introduction

A solid oxide fuel cell (SOFC) stack is generally composed of interconnects, sealing materials, and single cells [1]. Interconnects are used to provide electrical connection between the anode of one cell and the cathode of a neighboring cell, as well as to separate the anode side from the cathode side to avoid contact between air and fuel. With an operating temperature decreasing from 1000 °C to below 850 °C, the preference for metallic materials as interconnects for SOFC stacks has increased because of their low-cost, excellent thermal and electrical conductivities, and ease of fabrication compared with ceramics [2,3]. However, the high electric resistivity oxide scales formed on the surface of a metallic interconnect may increase the contact resistance between an interconnect and its adjacent components, thus creating a significant electrical power loss at the electrode/interconnect interface [4]. Moreover, the volatile chromium species, such as $CrO_3$ or $CrO_2(OH)_2$, from metallic interconnects have a tendency to be deposited at the triple-phase boundaries of the cathode/electrolyte/gas interface, thus resulting in the rapid degradation of the electrical properties of an SOFC cell [5–8]. Normally, a

* *Corresponding author*. Tel.: +86 87911363; fax: +86 86695470.
** *Corresponding author*. Tel.: +86 86685137; fax: +86 86695470.
E-mail addresses: guanwanbing@gmail.com (W. Guan), wgwang@nimte.ac.cn (W.G. Wang).
0360-3199/$ – see front matter 
http://dx.doi.org/10.1016/j.ijhydene.2013.10.094

**Table 1 – The nominal composition of SUS 430 stainless steel.**

| Elements/wt% | Fe | Cr | Ni | C | Mn | Si | P |
|---|---|---|---|---|---|---|---|
| SUS 430 | Bal | 16.14 | 0.044 | / | 0.209 | 0.279 | 0.028 |

reduction in interconnect oxidation rate and an inhibition of Cr diffusion are achieved by using two methods. The first method involves reducing the SOFC stack operating temperature. However, Gindorf [9] found that lowering the operation temperature from 900 °C to 750 °C does not result in a significant improvement in stack output performance. Thus, an increasing number of researchers have focused on the application of protective coatings acting as chromium diffusion barrier and oxide scale inhibitor [10].

At present, the most commonly used protective coating material for SOFC metallic interconnects are conductive perovskites; among which, lanthanum strontium manganite (LSM)-based perovskite materials have been extensively investigated because of their high electrical conductivity, thermal compatibility, and stability in an oxidizing environment [11–13]. In general, thermal spraying, particularly plasma spraying, is a highly flexible, cost-effective method for producing reproducible, durable, and thick ceramic coatings on metallic components [14–16]. Chu et al. [15] and Baik [16] applied LSM coating on stainless steel by plasma spraying, and the anti-oxidation ability of the substrate steel improved to a certain extent in both experiments. However, because of the ionic conducting nature of perovskites, the oxidation of metallic interconnect substrates and the formation of a chromia-rich subscale may not be significantly prevented [10]. Furthermore, the growth of chromia-rich scales can induce porosity at the alloy-scale interface, which can result in scale cracking and spallation under significant growth stresses [17]. The effectiveness of the LSM layer as a protective coating depends on the stability of the film and the adherence of the layer on the alloy substrate [12]. Therefore, to prolong the longevity of the LSM coating on metallic interconnects, the adherence of the coating to substrate should be improved. One approach to realize this condition is adding an interlayer between the LSM coating and the metallic interconnect. Numerous researchers have confirmed that metal and oxide coatings thermally converted from metal or metallic layers are promising coatings for SOFC interconnects because of their low-cost and easy fabrication through a wide range of techniques, such as plasma spraying and plating [18–22]. In 2011, Geng et al. [18] investigated the properties of magnetron sputtering Ni on SOFC metallic interconnects. They found that the sputtered Ni coating lowers the surface oxide scale area specific resistance (ASR) and acts as a Cr diffusion barrier because the NiO/$(Ni,Fe,Cr)_3O_4$ scale thermally converted from the sputtered Ni coating and Fe/Cr diffused from the steel

**Table 2 – The plasma spray parameters.**

| Current/A | Voltage/V | Ar flow rate/(L/H) | Powder feed rate/(L/H) |
|---|---|---|---|
| 600 | 55 | 1500 | 600 |

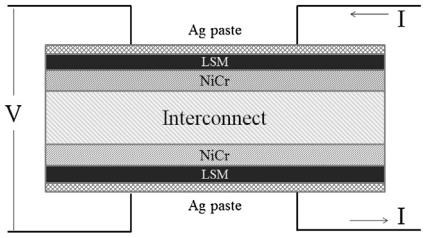


**Fig. 1 – Schematic illustration of area specific resistance measurements for coated alloy.**

substrate. Nie et al. [19] also applied Ni coating on stainless steel interconnects by plasma spraying and reducing the oxidation rate of the metallic substrate successfully. However, the Ni coatings mentioned in these previous studies have cracks and are likely to split from the interconnect substrate after oxidation. This phenomenon may be ascribed to thermal expansion coefficient (TEC) mismatch between Ni and the metallic substrate.

$Ni_{80}Cr_{20}$ alloy bridges the gap between pure elements and highly alloyed materials, such as Inconel 718 [23]. This alloy is currently the focus for thermal spraying metallic coating applications [24–26]. $Ni_{80}Cr_{20}$ alloy, which has good adherence to ceramic materials, can also be used in SOFC composite electrolyte [27] and in metal/ceramic composite coatings [28]. In the present study, plasma-sprayed $Ni_{80}Cr_{20}$/$(La_{0.75}Sr_{0.25})_{0.95}MnO_3$ coating on SUS 430 alloy was evaluated for planar SOFC interconnect application. The ASR of the coated alloy was investigated at 800 °C in air. A two-cell stack was also assembled and tested to evaluate the coating performance in an actual SOFC stack.

## 2. Experimental

Commercial SUS 430 stainless steel with an average thickness of 1.5 mm was used as an interconnect. The composition of the commercial alloy is listed in Table 1. Before plasma spraying, SUS 430 stainless steel was cut into 4 cm × 4 cm samples. The samples were ground to 600 grits with SiC sandpaper and cleaned in an acetone bath. The $(La_{0.75}Sr_{0.25})_{0.95}MnO_{3-\sigma}$ (LSM) power between 76 nm and

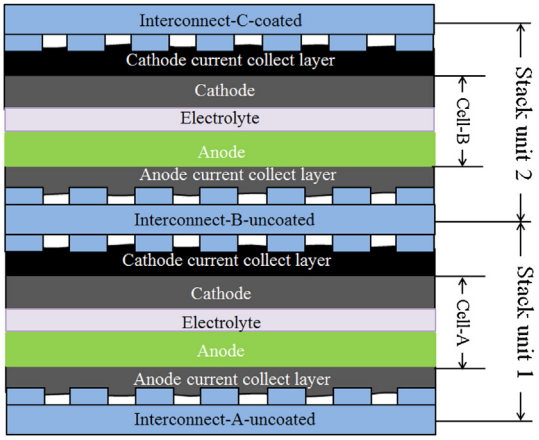


**Fig. 2 – Schematic diagram of 2-cell stack structure.**

**Table 3 – The 2-cell stack operation parameters.**

| External load (kPa) | Working temperature (°C) | Air flow rate/(SLM) | $H_2$ flow rate/(SLM) |
|---|---|---|---|
| 70 | 800 | 1.5 | 0.5 |

125 nm was prepared via Pechini route [29]. Commercial $Ni_{80}Cr_{20}$ powder (99.9% purity and 20 μm average particle size) produced by the Beijing Mining and Metallurgical Research Institute was directly used for spraying. Plasma spraying was conducted in an Ar atmosphere with the appropriate parameters listed in Table 2.

The ASRs of $Ni_{80}Cr_{20}/(La_{0.75}Sr_{0.25})_{0.95}MnO_3$ coated and bare samples were measured by a four-point method at 800 °C in air, as demonstrated in Fig. 1. Each surface of the samples was covered with a silver mesh with an active area of 15 $cm^2$. To ensure adequate electrical contact between the samples and the silver meshes, a constant mechanical load of 70 kPa was applied to the through-thickness direction. In the ASR test, a constant current of 2 A $cm^{-2}$ through the samples enabled voltage recording. The ASR of the samples could be calculated by the following equation:

$$\mathrm{ASR} = \frac{U \times S}{2I} \quad (1)$$

where $I$ is the charging current, $U$ is the output voltage, and $S$ is the active area. A factor of 2 was included to account for the measurement of the voltage across two sides. The phase structures and morphologies of the samples were identified by X-ray diffraction (XRD, D8 Advance) and scanning electron microscopy (SEM, FEI Quanta FEG 250), respectively.

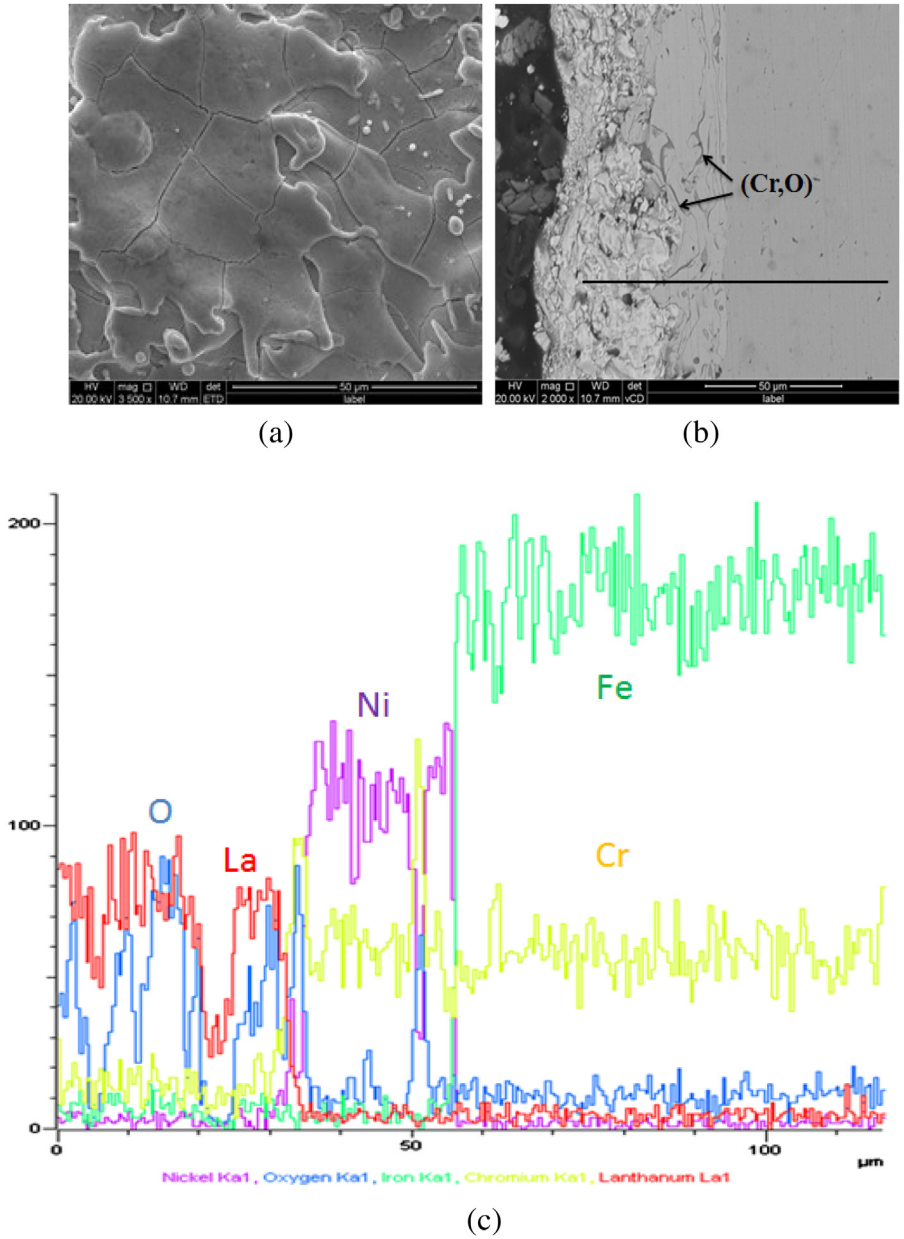


**Fig. 3 – SEM images of plasma sprayed coating on SUS 430 stainless steel; (a) surface image, (b) cross section image, (c) EDS image.**

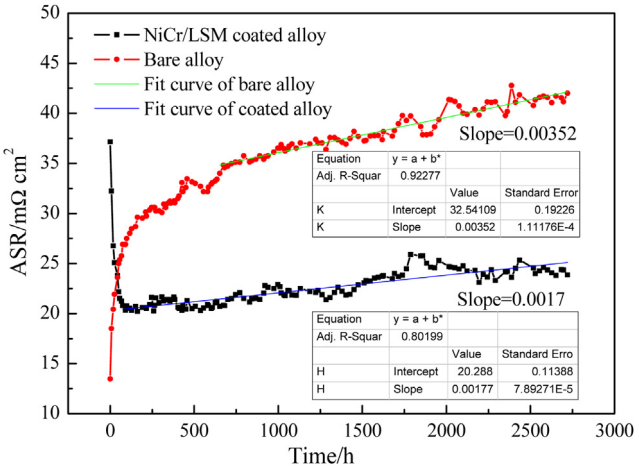


**Fig. 4 – ASRs versus time for bare steel and SUS 430 stainless steel with NiCr/LSM coating at 800 °C in air.**

A two-cell stack was assembled to evaluate the performance of the interconnect with NiCr/LSM coating in an actual stack according to the structure shown in Fig. 2. The stack comprised three pieces of SUS 430 interconnects (designated as interconnects A, B, and C) and two pieces of SOFC cells (designated as cells A and B), in which the size of the interconnect and the cell is 10 cm × 10 cm. The cells used in the stack were typical Ni-YSZ/YSZ/LSM anode-supported SOFCs with an active area of 63 $cm^2$. These cells were manufactured by the Ningbo Institute of Material Technology and Engineering, China. All cells were screen printed. A 100 μm thick LSM served as the cathode current collecting layer, whereas a 100 μm thick NiO acted as the anode current collecting layer. Interconnects A and B were uncoated, and interconnect C was coated with dual-layer NiCr/LSM. Cell A, together with interconnects A and B, was designated as stack repeating unit 1. Cell B, along with interconnects B and C, was designated as stack repeating unit 2. After assembly, the stack was placed in a furnace and heated to 800 °C. Then, it was tested with pure $H_2$ as fuel and air as cathode gas. The stack operation parameters are listed in Table 3. The effect of $Ni_{80}Cr_{20}$/$(La_{0.75}Sr_{0.25})_{0.95}MnO_3$ interconnect coating on stack performance was analyzed using the corresponding I–V and V–T curves.

## 3. Results and discussion

The morphologies of the sprayed NiCr/LSM coating before oxidation were observed via SEM, as shown in Fig. 3. The surface (Fig. 3a) and cross-section (Fig. 3b) images showed that the sprayed NiCr/LSM layer was continuous with a uniform thickness of approximately 50 μm, and bonded well to the alloy substrate. The cracks on the surface of the coating layer might be caused by the shrinkage of the thin film during the cooling stage after the plasma spraying process. The energy dispersive X-ray (EDX) spectrometry line scan of the coating cross section (Fig. 3a) indicated that small quantities of chromia exited in the NiCr layer. This phenomenon might have occurred during the spraying process.

In general, when oxides are formed on the surface of alloys, the ASR can be obtained by the following equation [3]:

$$ASR = \rho \cdot \chi = \rho \cdot \sqrt{2Kt} \quad (2)$$

where $\rho$ is the resistivity of the oxides formed on the surface, $X$ is the thickness of the oxides, and $K$ is the scaling constant.

The ASRs of the bare alloy and the alloy with NiCr/LSM coating after oxidation in air at 800 °C for 2800 h are shown in Fig. 4. As shown in the figure, the initial ASR value of the uncoated SUS 430 alloy was 10 mΩ $cm^2$, and this value increased over time to approximately 42 mΩ $cm^2$ after oxidation. The ASR value of the uncoated SUS 430 alloy increased rapidly during the initial stage as a result of the increasing thickness of the oxide scale. The resistance value became stable with increasing duration, thus describing a parabolic growth. The thickness of the oxide scale increased at a parabolic rate, and the alloy oxidation process followed the kinetics described in Equation (2). By contrast, the ASR of the alloy with NiCr/LSM coating decreased sharply at the initial stage because of the improvement of interface bonding between the NiCr/LSM

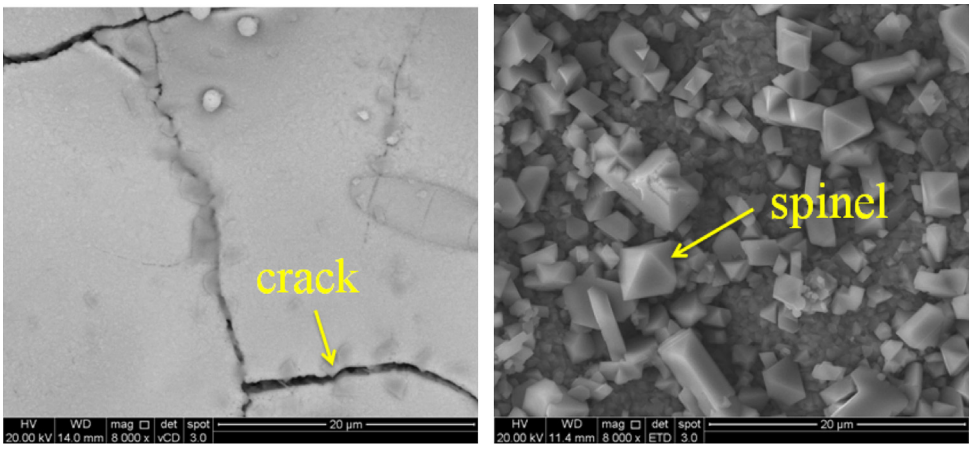


**Fig. 5 – SEM surface images of (a) coated SUS 430 stainless steel and (b) bare steel after holding at 800 °C for 2800 h.**

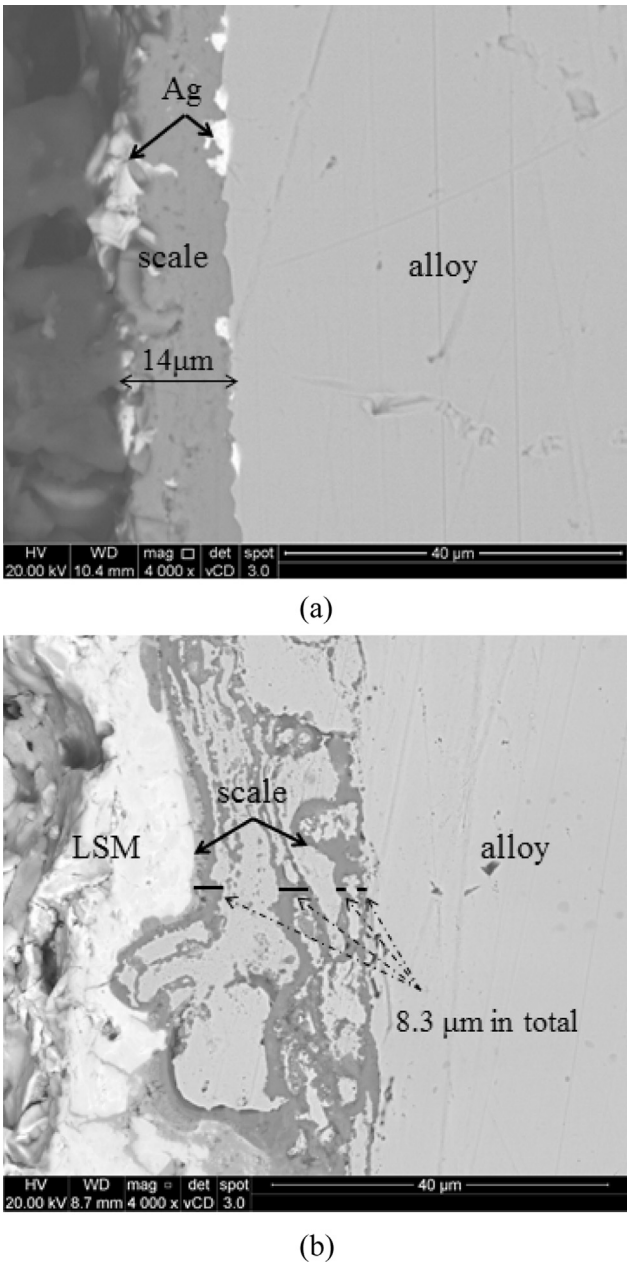


**Fig. 6 – Cross-section SEM images of (a) bare SUS 430 and (b) SUS 430 with NiCr/LSM coating after oxidation at 800 °C for 2800 h in air.**

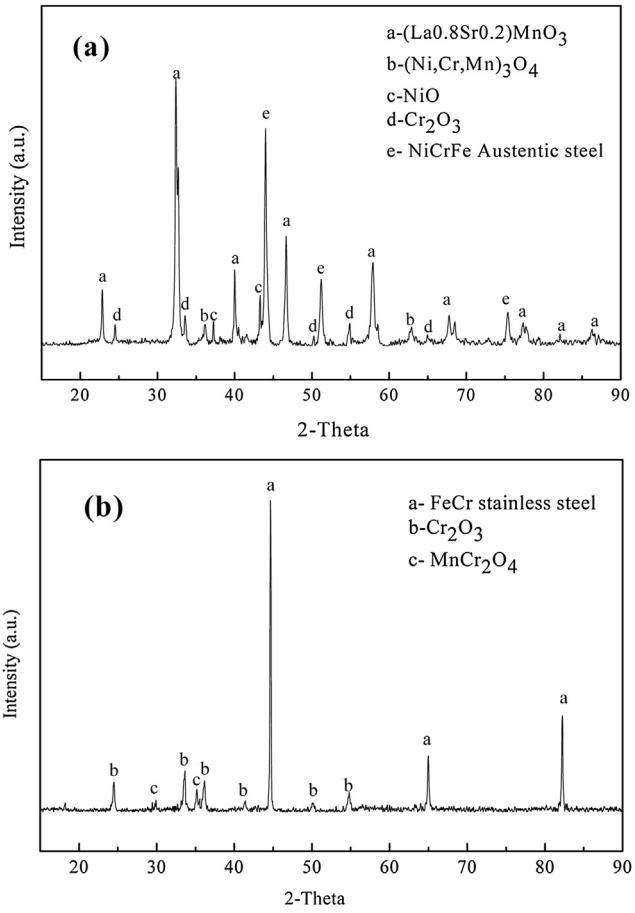


**Fig. 7 – XRD patterns of (a) coated alloy and (b) bare alloy after holding at 800 °C for 2800 h.**

layer and the substrate alloy. After oxidation at 800 °C for 2800 h, the ASR of SUS 430 alloy with NiCr/LSM coating was approximately 25 mΩ $cm^2$, which was 40% lower than that of the bare alloy. Moreover, the ASR increasing rate of the coated alloy was more stable, which demonstrates a linear characteristic.

At present, the target durability required for the metallic interconnect for SOFC includes an operating time of 40,000 h and an ASR value below 100 mΩ $cm^2$ [3]. From the linear fit results in Fig. 8, the ASR increasing rate of SUS 430 alloy with NiCr/LSM coating was 0.0017 mΩ $cm^2$/h. The ASR of the coated alloy was estimated to be 90 mΩ $cm^2$ after oxidizing at 800 °C for 40,000 h. Thus, preliminary results suggested that the NiCr/LSM coating could reduce the high temperature ASR of SUS 430 alloy for SOFC interconnect application.

The surface morphologies of the samples after oxidation at 800 °C for 2800 h are illustrated in Fig. 5. Numerous irregularly shaped grains formed on the bare alloy after oxidation. The NiCr/LSM coating on the alloy surface was uniform. However, a number of macro cracks were observed on the surface of the LSM coating. These cracks were caused by thin film shrinkage during the plasma spraying process and did not go through the entire dual layer after oxidation. The cross-section structure of the coating was also observed by SEM. As shown in Fig. 6, the thickness of the oxide scale formed on the coated SUS 430 alloy was approximately 8.3 μm. This scale was thinner than the scale formed on the bare alloy (approximately 14 μm), thus indicating that the NiCr/LSM coating could significantly reduce the growth rate of the scale formed on the alloy surface.

In general, the electrical conductivity of metallic interconnects depends more on the electrical conductivity of the oxide scale that formed on the surface after oxidation than the metal itself [4]. As shown in Fig. 6a, the scale thickness of the bare SUS 430 alloy after oxidation was significantly greater than that of the alloy with NiCr/LSM coating. The conductivity of NiCr/LSM coating was higher than that of Cr-rich oxide;

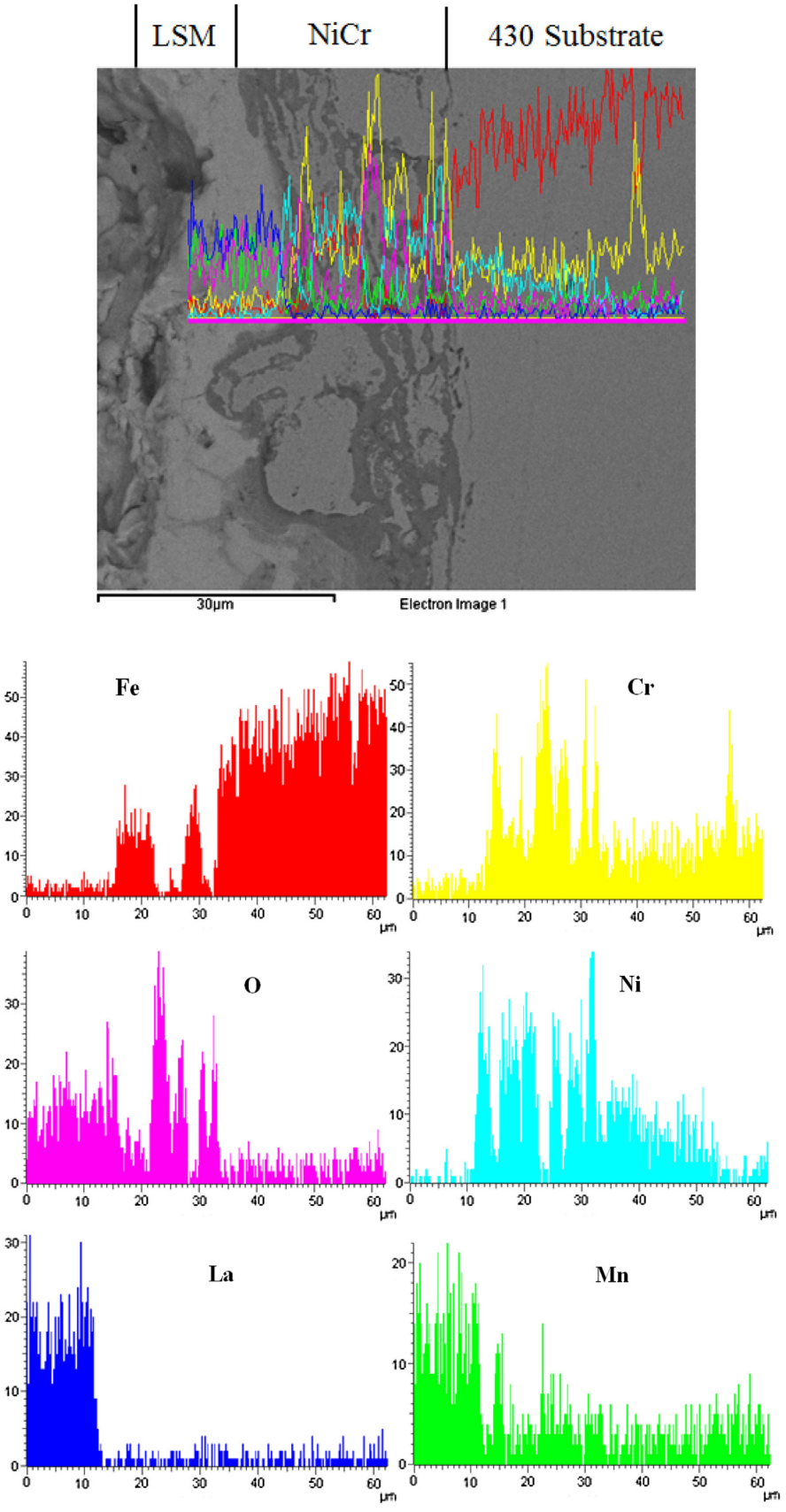


**Fig. 8 – Cross-section EDX line scans of SUS 430 stainless steel with NiCr/LSM coating after oxidation at 800 °C for 2800 h in air.**

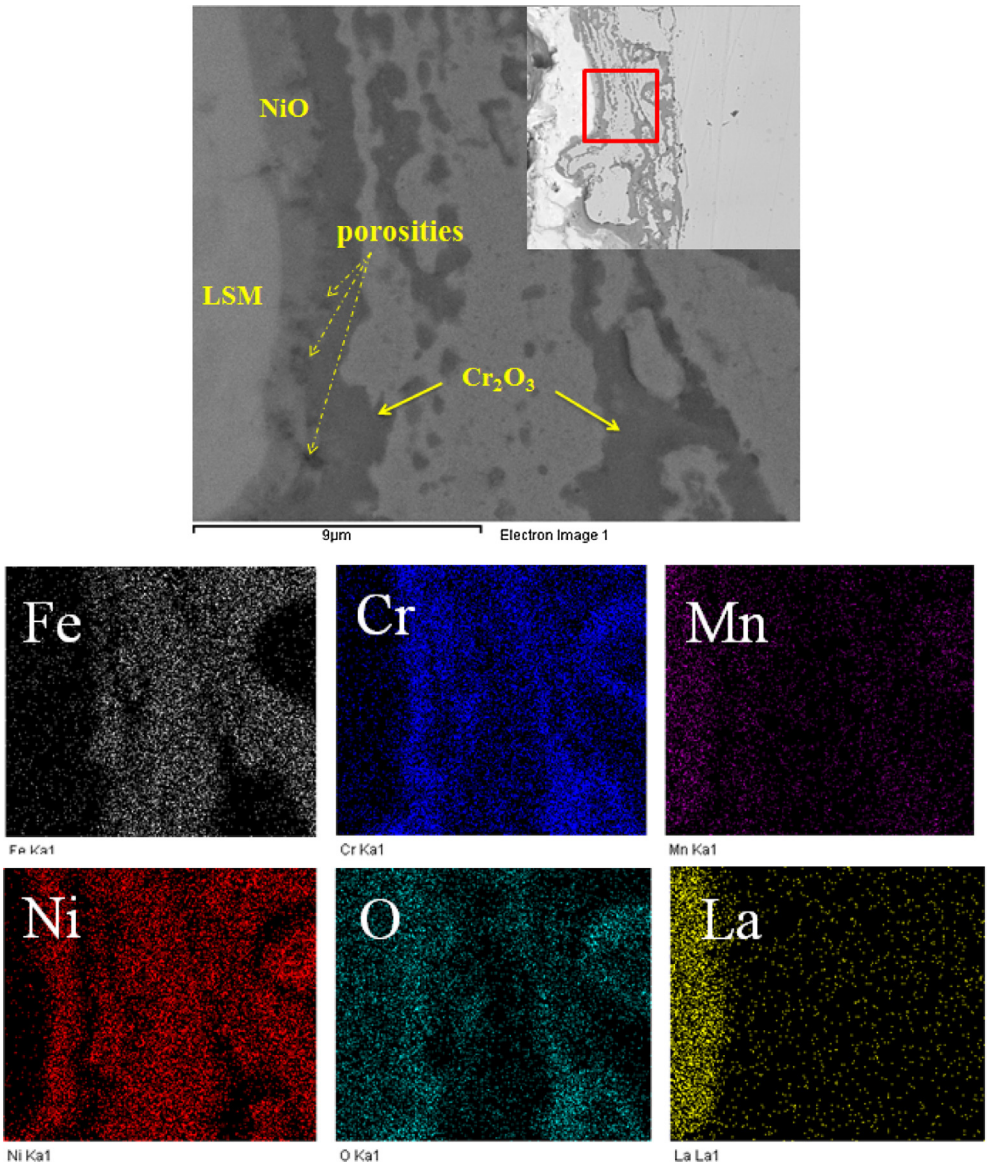


**Fig. 9 – Cross-section elemental distribution of the NiCr/LSM coated SUS 430 alloy after oxidation at 800 °C for 2800 h in air.**

thus, the coated alloy had a lower high-temperature ASR, which coincides with the results demonstrated in Fig. 4.

The phase structures of the oxide scales formed on the samples after oxidation were identified using XRD, and the results are shown in Fig. 7. The oxides formed on the bare alloy mainly comprised $Cr_2O_3$ and $MnCr_2O_4$. By contrast, the oxides including NiO, $(Ni,Cr,Mn)_3O_4$, and $Cr_2O_3$ were thermally developed on the alloy with NiCr/LSM coating. The oxide structure formed on the NiCr/LSM coated alloy was different from that formed on the uncoated alloy. A signature of the Fe–Cr–Ni austenitic region was also detected. In general, Ni–Cr-base austenitic alloys demonstrate a higher TEC than body-centered cubic ferritic stainless steel, which typically have a TEC of 13.0–14.9 $\times$ $10^{-6}$ $K^{-1}$ [30]. Thus, crack formation or crack propagation may occur during oxidation because of TEC mismatch. In contrast to what is expected, the austenitic phase did not cause spallation or other thermo-mechanical issues during isothermal oxidation and the cooldown processes of the specimens.

The SEM cross sections with an element line scan of the SUS 430 alloy with NiCr/LSM coating after oxidation are presented in Fig. 8. As shown in the figure, the internal oxidation zone was mainly located in the NiCr layer, and insignificant quantities of Fe had diffused into the NiCr layer. Combined with the cross-section image of the as-sprayed coating (Fig. 3b), the location of chromia particles in Fig. 3b seemed to correspond to the location of the chromia scale after the degradation test (Fig. 6b). The original chromia particles in the as-sprayed NiCr layer could serve as active sites for oxidation. According to the XRD results in Fig. 7, Fe diffused from the SUS 430 substrate to the NiCr layer and formed a Fe–Cr–Ni austenitic region. The slow diffusion of Cr in the austenitic region reduced the growth rate of the chromia scale, and thus, was beneficial to electrical performance [23].

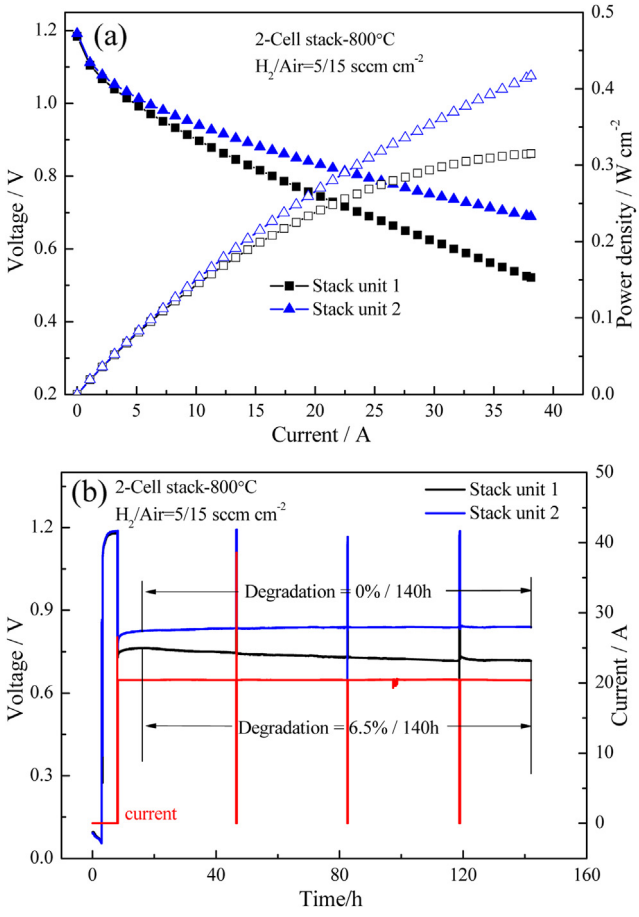


**Fig. 10 – I–V curves and degradation curves of Unit cells: (a) I–V curves and (b) degradation curves.**

The cross-section details of the NiCr/LSM-coated alloy with element distribution are shown in Fig. 9. The oxide scale on the alloy with NiCr/LSM coating comprised a dual-layer oxide structure with an outer layer of Ni-rich oxide and an inner layer of Cr-rich oxide. From the combined results of XRD (Fig. 7) and EDX (Fig. 8), the outer layer was found to be NiO, whereas the inner layer was mainly $Cr_2O_3$. The Cr-rich oxide appeared immediately below the NiO scale, thus showing that $Cr_2O_3$ was thermodynamically more stable than NiO, and that NiO and $Cr_2O_3$ were insoluble. Several degrees of porosity (Fig. 9) existed in the interface between the NiO and $Cr_2O_3$ scales. This varying porosity most likely occurred because of the TEC mismatch between the two scales [31]. However, the outer layer seemed to exhibit improved scale adhesion to the LSM layer.

A small amount of (Ni, Cr, Mn)$_3O_4$ spinels were found beneath the NiO layer. These spinels could inhibit the evaporation and out-diffusion of Cr. Therefore, the plasma-sprayed $Ni_{80}Cr_{20}/(La_{0.75}Sr_{0.25})_{0.95}MnO_3$ dual-layer coating exhibited good adherence to SUS 430 stainless steel at SOFC working temperatures and also acted as a Cr diffusion barrier.

The I–V curves and the degradation results of a two-cell stack at 800 °C are shown in Fig. 10. The average open circuit voltages of stack repeating units 1 and 2 were more than 1.15 V (Fig. 10a), thus indicating good sealing performance in the stack. The maximum output current and power density of stack repeating unit 2 were 38 A and 0.45 W cm$^{-2}$, respectively. The maximum output power density of stack repeating unit 1 was only 0.32 W cm$^{-2}$, which was 0.13 W cm$^{-2}$ lower than that of stack repeating unit 2. These results indicated that NiCr/LSM coating could effectively improve SOFC stack output performance. After each I–V test curve was collected, the stack was discharged at a 20 A (0.36 A cm$^{-2}$) constant current with a fuel utilization of approximately 87%. As shown in Fig. 10b, the degradation of stack repeating unit 1 after operating for 140 h reached 6.5%, whereas stack repeating unit 2 exhibited no degradation. From the combined results of the ASR test, the degradation of stack repeating unit 1 was derived from the scale growth on the bare SUS 430 surface, which increased contact resistance between the interconnect and the cathode. By contrast, stack repeating unit 2 was estimated to have a much lower contact resistance at the cathode side because of the improved anti-oxidation ability of NiCr/LSM-coated interconnects, and the similar nature of the cathode material and the outer LSM layer of coating. By considering these results, the $Ni_{80}Cr_{20}/(La_{0.75}Sr_{0.25})_{0.95}MnO_3$ dual-layer coating reduced the oxidation rate of SUS 430 stainless steel used in SOFC interconnects and inhibited Cr out-migration from the steel substrate. During the SOFC operation, the $Ni_{80}Cr_{20}/(La_{0.75}Sr_{0.25})_{0.95}MnO_3$-coated interconnect improved stack output performance and durability, thus prolonging the service life of the SOFC.

## 4. Conclusions

$Ni_{80}Cr_{20}/(La_{0.75}Sr_{0.25})_{0.95}MnO_3$ dual-layer coating was plasma sprayed on SUS 430 alloy for intermediate SOFC interconnect application. The coating adhered well to the SUS 430 alloy before and after oxidation. The ASR value of the coated alloy was 25 mΩ cm$^2$ after oxidation at 800 °C in the air for 2800 h, which was 39% lower than that of bare alloy. The NiO/(Ni, Cr, Mn)$_3O_4$/$Cr_2O_3$ scale structure could effectively inhibit Cr out-migration.

In the actual stack test, the maximum output power density of the stack unit increased from 0.32 W cm$^{-2}$ to 0.45 W cm$^{-2}$ because of the application of NiCr/LSM coating. The degradation rate of the stack unit without coating was 4.4%/100 h at a current of 20 A, whereas the stack unit with NiCr/LSM coating exhibited no degradation. These results indicated that $Ni_{80}Cr_{20}/(La_{0.75}Sr_{0.25})_{0.95}MnO_3$ dual-layer coating was remarkable as a protective coating for SOFC metallic interconnects.

## REFERENCES

[1] Wen TL, Wang D, Tu HY, Chen M, Lu Z, Zhang Z, et al. Research on planar SOFC stack. Solid State Ionics 2002;152:399–404.
[2] Fergus JW. Metallic interconnects for solid oxide fuel cells. Mat Sci Eng A-Struct 2005;397:271–83.
[3] Wu JW, Liu XB. Recent development of SOFC metallic interconnect. J Mater Sci Technol 2010;26:293–305.

[4] Wu W, Wang GL, Guan WB, Zhen YF, Wang WG. Effect of contact method between interconnects and electrodes on area specific resistance in planar solid oxide fuel cells. Fuel Cells 2013;13:743–50.
[5] Jiang SP, Zhang JP, Apateanu L, Foger K. Deposition of chromium species at Sr-doped $LaMnO_3$ electrodes in solid oxide fuel cells, I. Mechanism and kinetics. J Electrochem Soc 2000;147:4013–22.
[6] Jiang SP, Zhang JP, Zheng XG. A comparative investigation of chromium deposition at air electrodes of solid oxide fuel cells. J Eur Ceram Soc 2002;22:361–73.
[7] Jiang SP, Zhang JP, Zhen YD. Early interaction between Fe-Cr alloy metallic interconnect chromium species at Sr-doped $LaMnO_3$ cathodes for solid oxide fuel cell. J Mater Res 2005;20:747–58.
[8] Jiang SP, Zhang JP, Foger K. Deposition of chromium species at Sr-doped $LaMnO_3$ electrodes in solid oxide fuel cells: III. Effect of air flow. J Electrochem Soc 2001;148:C447–55.
[9] Gindorf C, Singheiser L, Hilpert K. Chromium vaporisation from Fe-Cr base alloys used as interconnect in fuel cells. Steel Res 2001;72:528–33.
[10] Shaigan N, Qu W, Ivey DG, Chen WX. A review of recent progress in coatings, surface modifications and alloy developments for solid oxide fuel cell ferritic stainless steel interconnects. J Power Sources 2010;195:1529–42.
[11] Pyo SS, Lee SB, Lim TH, Song RH, Shin DR, Hyun SH, et al. Characteristic of $(La_{0.8}Sr_{0.2})_{0.98}MnO_3$ coating on Crofer22APU used as metallic interconnects for solid oxide fuel cell. Int J Hydrogen Energ 2011;36:1868–81.
[12] da Conceição L, Dessemond L, Djurado E, Souza MMVM. $La_{0.7}Sr_{0.3}MnO_3$-coated SS444 alloy by dip-coating process for metallic interconnect supported Solid Oxide Fuel cells. J Power Sources 2013;241:159–67.
[13] Chu CL, Lee J, Lee TH, Chen YN. Oxidation behavior of metallic interconnect coated with La–Sr–Mn film by screen painting and plasma sputtering. Int J Hydrogen Energ 2009;34:422–34.
[14] Puranen J, Lagerbom J, Hyvarinen L, Mantyla T, Levanen E, Kylmalahti M, et al. Formation and structure of plasma sprayed manganese-cobalt spinel coatings on preheated metallic interconnector plates. Surf Coat Tech 2010;205:1029–33.
[15] Chu C, Wang J, Lee S. Effects of $La_{0.67}Sr_{0.33}MnO_3$ protective coating on SOFC interconnect by plasma-sputtering. Int J Hydrogen Energ 2008;33:2536–46.
[16] Baik KH. Effects of plasma-sprayed $La_{0.7}Sr_{0.3}MnO_3$ coating on thermally grown oxide scale and electrical conductivity of Fe–Cr interconnect for SOFCs. J Electrochem Soc 2013;160:F560–5.
[17] Wang KL, Liu YJ, Fergus JW. Interactions between SOFC interconnect coating materials and chromia. J Am Ceram Soc 2011;94:4490–5.
[18] Geng SJ, Wang Q, Wang W, Zhu SL, Wang FH. Sputtered Ni coating on ferritic stainless steel for solid oxide fuel cell interconnect application. Int J Hydrogen Energ 2012;37:916–20.
[19] Nie HW, Wen TL, Tu HY. Protection coatings for planar solid oxide fuel cell interconnect prepared by plasma spraying. Mater Res Bull 2003;38:1531–6.
[20] Nielsen KA, Dinesen AR, Korcakova L, Mikkelsen L, Hendriksen PV, Poulsen FW. Testing of Ni-plated ferritic steel interconnect in SOFC stacks. Fuel Cells 2006;6:100–6.
[21] Geng SJ, Qi SJ, Zhao QC, Zhu SL, Wang FH. Electroplated $Ni–Fe_2O_3$ composite coating for solid oxide fuel cell interconnect application. Int J Hydrogen Energ 2012;37:10850–6.
[22] Palcut M, Mikkelsen L, Neufeld K, Chen M, Knibbe R, Hendriksen PV. Efficient dual layer interconnect coating for high temperature electrochemical devices. Int J Hydrogen Energ 2012;37:14501–10.
[23] Hupf T, Cagran C, Kaschnitz E, Pottlacher G. Thermophysical properties of $Ni_{80}Cr_{20}$. Thermochim Acta 2009;494:40–4.
[24] Zois D, Wentz T, Dey R, Sampath S, Weyant CM. Simplified model for description of HVOF NiCr coating properties through experimental design and diagnostic measurements. J Therm Spray Techn 2013;22:299–315.
[25] Ak NF, Tekmen C, Ozdemir I, Soykan HS, Celik E. NiCr coatings on stainless steel by HVOF technique. Surf Coat Tech 2003;174:1070–3.
[26] Chatha SS, Sidhu HS, Sidhu BS. High-temperature behavior of a NiCr-coated T91 boiler steel in the platen superheater of coal-fired boiler. J Therm Spray Techn 2013;22:838–47.
[27] Liu FJ, Fang MH, Huang ZH, Liu YG, Huang SF, Min X, et al. Preparation and mechanical properties of $NiCr–Al_2O_3–ZrO_2$(8Y) ceramic composites. Mat Sci Eng A-Struct 2012;554:1–5.
[28] Xie ZQ, Wang HJ, Lu F, Zhang Y. Study on $NiCr-Cr_3C_2$ deposition efficiency of two supersonic spraying. Proced Earth Plan Sc 2011;2:122–6.
[29] Wang JX, Tao YK, Shao J, Wang WG. Synthesis and properties of $(La_{0.75}Sr_{0.25})_{0.95}MnO_{3\pm\delta}$ nano-powder prepared via Pechini route. J Power Sources 2009;186:344–8.
[30] Yang Z, Xia GG, Stevenson JW. Evaluation of Ni–Cr-base alloys for SOFC interconnect applications. J Power Sources 2006;160:1104–10.
[31] Zhu WZ, Deevi SC. Development of interconnect materials for solid oxide fuel cells. Mater Sci Eng A 2003;348:227–43.